COBEM 2023 27TH INTERNATIONAL CONGRESS OF MECHANICAL ENGENEERING

ABCM Brazilian Society of Mechanical Sciences and Engineering
27th ABCM International Congress of Mechanical Engineering
December 04-08, 2023, Florianópolis-SC, Brazil

COB-2023-1359
Performance prediction of a novel compact magnetocaloric wine cooler

Natália Maleski de Sá
natalia.sa@polo.ufsc.br
Glenda de Melo Luz
glenda.luz@polo.ufsc.br
Alan Tihiro Dias Nakashima
alan.nakashima@polo.ufsc.br
Elias Pagnan
elias.pagnan@polo.ufsc.br
Anderson Lorenzoni
anderson.lorenzoni@polo.ufsc.br
Guilherme Fidelis Peixer
guilherme.peixer@polo.ufsc.br
Jaime Andrés Lozano
jaime@polo.ufsc.br
Jader Riso Barbosa Jr.
jrb@polo.ufsc.br

Polo - Research Laboratories for Emerging Technologies in Cooling and Thermophysics, Department of Mechanical Engineering
Federal University of Santa Catarina, Florianópolis, SC, 88040-900, Brazil

Abstract. *The goal of the PoloMag project is to develop a novel, fully integrated plug-and-play magnetocaloric refrigerator capable of controlling the temperature of a 31-bottle wine cooler cabinet between 10 and 18°C in an ambient temperature of 25°C, and with a thermodynamic performance comparable to that of a vapor compression system operating the same cabinet. This work presents the main design aspects and numerical results of the second version of the magnetocaloric wine cooler designed by PoloMag. Optimized for a target cabinet temperature of 12°C, the magnetocaloric wine cooler is expected to be 116% more efficient than a commercially available vapor compression system tested in our group and 238% more efficient than our previous magnetocaloric wine cooler prototype, in terms of the second-law efficiency. The results also show that the magnetocaloric wine cooler can reach a maximum overall performance for a cabinet temperature of 13°C and an operating frequency of 0.25 Hz, with a second-law efficiency of 6.77% and a coefficient of performance of 1.46.*

Keywords: *magnetocaloric refrigeration, thermal system design, numerical analysis, performance assessment*

1. INTRODUCTION

Magnetocaloric refrigeration (MR) is a not-in-kind cooling technology based on the magnetocaloric effect (MCE), a thermal response exhibited by certain magnetocaloric materials (MCM) when subjected to a changing magnetic field. MR exploits the MCE in a regenerative thermodynamic cycle to transfer heat from a low-temperature environment to a high-temperature one by means of magnetic work. MR stands as an upcoming alternative to the vapor compression (VC) technology in certain domains, specially for near room-temperature applications, for its potential to be more efficient (Qian *et al.*, 2016). Essentially, it replaces the compression/expansion of the refrigerant fluid and its liquid-vapor phase-change refrigerating effect by the magnetization/demagnetization of a solid MCM refrigerant going through a magnetic phase transition and exhibiting the MCE.

A state-of-the-art magnetocaloric refrigerator is mainly composed of: (i) a magnetic circuit (MC), responsible for generating the magnetic field and its variation on the MCM; (ii) an active magnetic regenerator (AMR), a porous matrix of MCM responsible for providing the cooling capacity; (iii) a hydraulic circuit (HC), responsible for displacing the fluid that acts as a thermal exchange medium between the MCM and the thermal reservoirs, and for synchronizing the fluid flow in each regenerator with the rotation of the magnet; (iv) heat exchangers (HEx) and fans, responsible for enabling the heat exchange between the thermal fluid and the thermal reservoirs. The magnetic field sources used in MR are based on permanent magnets, thus not requiring a continuous energy source to generate the field, which could reduce overall system energy consumption. The application of solid MCM as refrigerants and water-based thermal fluids eliminates problems with direct emissions and risks of accidents involving the flammability and toxicity of some refrigerant fluids.

Furthermore, despite the lower specific refrigerating effect of current MCM, the MCE is thermodynamically reversible, which favors the potential to achieve higher efficiencies.

Nevertheless, the distance between conception and achievement of these advantages is still substantial, and significant work is still required to bring this technology to the market. Many lab-scale prototypes have been designed and commissioned worldwide, including magnetocaloric refrigerators (Tura and Rowe, 2011; Engelbrecht *et al.*, 2012; Jacobs *et al.*, 2014; Eriksen *et al.*, 2015; Aprea *et al.*, 2016; Nakashima *et al.*, 2021; Peixer *et al.*, 2023) and heat pumps (Dall'Olio *et al.*, 2021), with capacities ranging from 25 to 2000 W. Most of them, however, utilize electrical heaters and thermal baths to simulate heat source and sink temperatures. Consequently, the cooling capacity and temperature span values reported are specific to the AMR cycle rather than the entire system. This neglects the impact of heat exchanger effectiveness, fan power dissipation and cabinet losses in the system performance. Additionally, the losses of pump, motor and valves are often overlooked in the evaluation procedures of system performance (Peixer *et al.*, 2023), giving rise to discrepancies among performance figures and preventing a comprehensive analysis of the readiness level of the magnetocaloric technology.

Within this scenario, the PoloMag group (POLO Labs - UFSC) emerged as a research team focused on establishing MR as a viable technology, developing several relevant works and prototypes in the past decade. Among them, Nakashima *et al.* (2021) presented the first version of the MR wine cooler (MR1)[1], one of the first MR prototypes in literature to consider a cabinet and real heat exchangers in the performance assessment (De Sá *et al.*, 2023b). MR1 was able to reach a minimum cabinet temperature of 10.8°C, but with a very high energy consumption. Later, Nakashima *et al.* (2022) proposed a system-level model able to predict the unsteady- and steady-state behavior and performance metrics of magnetic refrigerators. De Sá *et al.* (2023b) carried out a performance comparison of MR1 with a VC refrigerating system operating the same wine cooler cabinet (VC1), showing that the wine cooler had a higher performance when operated by VC1. The work revealed some of the gaps between both cooling technologies and prompted several improvements suggestions for the MR1 prototype. More recently, De Sá *et al.* (2023a) introduced the conceptual design and optimization of a second version of the MR wine cooler using the model of Nakashima *et al.* (2022), considering several system configurations and aiming at minimizing the magnet mass and maximizing the coefficient of performance (COP).

The present work advances and details the design aspects of the novel compact MR wine cooler – the MR2, showing the main features of each subsystem. Numerical results in the form of performance maps are presented and discussed. The subsystems are evaluated by their contributions to the system power consumption. Further analysis include the performance comparison between MR1, VC1 and MR2 in terms of COP and second-law efficiency ($\eta_{2\mathrm{nd}}$).

2. MAGNETIC WINE COOLER DESIGN

The kickoff of the MR2 design was the experimental results achieved by MR1 and its thermodynamic comparison with the experimental results of VC1. De Sá *et al.* (2023b) showed that MR1 reached about 70% of the COP of VC1, presenting a 94% higher energy consumption operating between the same thermal reservoirs. They also showed that the main source of irreversibility in MR1 was the pumping system, having a great power requirement in order to compensate for the low refrigerating effect of the solid refrigerant employed, the gadolinium (Gd) and gadolinium alloys (Gd-Y). Additionally, the authors pointed out how bulkier the MR1 system was compared to VC1, as the magnetic circuit of MR1 was almost twice heavier (17.2 kg) than the compressor of VC1 (9 kg), suggesting that further optimization should consider the reduction of the system volume.

With those guidelines, the main goals of the MR2 design were to address the limitations of the MR1 and to outperform VC1. The design methodology was based on the system model of Nakashima *et al.* (2022) coupled with a genetic algorithm-based optimization routine, aiming at maximizing the COP of the system while minimizing the magnet mass employed in the magnetic circuit. This section presents the detailed features of the final configuration of MR2 and its subsystems.

2.1 Magnetic circuit

The MC of MR2 has an axial configuration based on a Halbach double-C arrangement (Kaneko *et al.*, 2019; Pagnan, 2022), schematically presented in Fig. 1. The MC is composed of four regions of hard magnetic material, two regions of soft magnetic material and two regions of air gap. The regions of hard magnetic material are composed of two different classes of NdFeB magnet blocks: the *central* magnets and the *lateral* concentrator magnets. The central magnets are responsible for generating the magnetic field in a specific direction. The lateral concentrator magnets are responsible for reducing border effects and increasing the intensity of the magnetic field in the air gap. The regions of soft magnetic material are composed of 1020 steel and are responsible for guiding the magnetic flux lines and closing the magnetic circuit. Lastly, the regions of air gap are the regions with a high magnetic field where the regenerators are positioned.

The design of the MC focused on minimizing the mass of Nd-Fe-B in order to develop a compact system. Furthermore, the width and depth of the MC were limited by the width and depth of the cabinet. The Nd-Fe-B blocks were selected

[1] A video illustrating the main features of the MR1 system is available online in `https://www.youtube.com/watch?v=y56ApAvZDoA`.

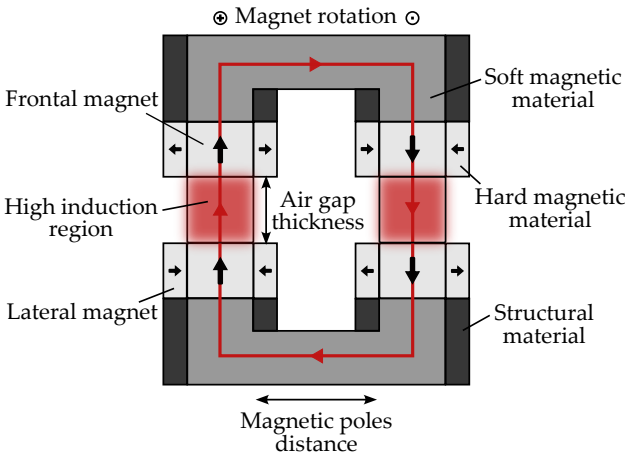

Figure 1. Schematic frontal view of the MC.

according to commercial availability. The rotary motion of the MC is set by a stepper motor and gears, and the efficiency of the transmission system is estimated at 80%. The main parameters of the MC design are presented in Tab. 1.

Table 1. Main parameters of the MC.

Parameter	Value
Maximum induction	0.87 T
Magnet mass	8.85 kg
Air gap thickness	21 mm
Magnetic poles distance	210 mm

2.2 Active magnetic regenerator

The AMR consists of trapezoidal housings filled with spheroidal particles of solid refrigerant. Figure 2 presents the superior view (schematic) of the AMR. The AMR is arranged as a disk divided into 8 individual regenerators beds, through which fluid flows in the tangential direction. The length of each AMR bed is given by a fraction of the available arc swept by the rotation movement of the MC minus the length spared for the hydraulic adapters. The height of the AMR is given by the height of the air gap minus the thickness of the AMR housing and an air layer spared for assembly purposes.

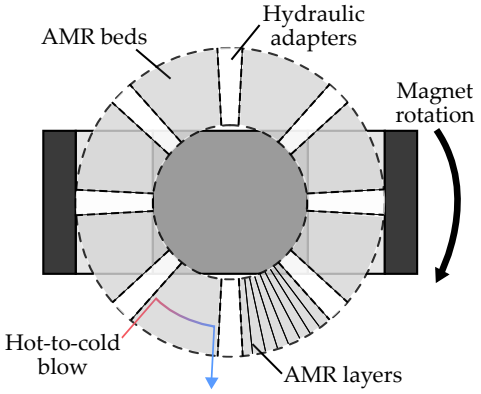

Figure 2. Schematic superior view of the AMR set.

The AMR casing is made of polyacetal and the covers are made of stainless steel. The solid refrigerant layers are separated by stainless steel frames with wire meshes. Limitations in the AMR design were due to the availability of MCM in the Polo Labs. The AMR is filled with a hybrid combination of Gd, Gd-Y and the Lanthanum-Iron-Silicon (La-Fe-Si) alloys, divided into layers with different Curie temperatures. The Curie temperature of a MCM is the temperature in which the MCE exhibits a peak in magnitude, and thus the AMR layers are set up with a temperature profile consistent with that underwent by the thermal fluid flowing through the regenerators. The Curie temperature profile was designed

for a target temperature of 12°C and ranges from 4.0 to 24.9°C. A total of 275 g of MCM is allocated in each regenerator, of which 65% is Gd and Gd-Y and 35% is La-Fe-Si. Table 2 presents the main parameters of the AMR.

Table 2. Dimensions and parameters of the active magnetic regenerators.

Parameter	Value
No. of AMR beds	8
Air layer thickness	1 mm
Housing thickness	1.5 mm
Adaptors length	30 mm
AMR bed length	70.5 mm
AMR bed width	51 mm
AMR height	16.7 mm
Porosity	0.40
Total mass of MCM	2.20 kg

2.3 Hydraulic circuit

The HC of MR2 is responsible for generating the flow of the thermal fluid through the AMR and the HEx and for synchronizing the fluid flow in each regenerator pair with the MC rotation. The HC is composed of solenoid valves, check valves, a pumping system and the tubing. Figure 3 presents the HC scheme of the MR2. Two 2/2-way solenoid valves control a pair of regenerators, managing the inlet and outlet of the fluid flowing through the AMR at the hot end. Sixteen check valves control the flow direction through the AMR at the cold end, establishing unidirectional flow through the cold HEx. This configuration ensures continuous flow through the HEx and oscillating flow through the AMR beds, and was selected for its favorable trade-off between overall energy performance and cost (Cardoso *et al.*, 2016; Nakashima *et al.*, 2021).

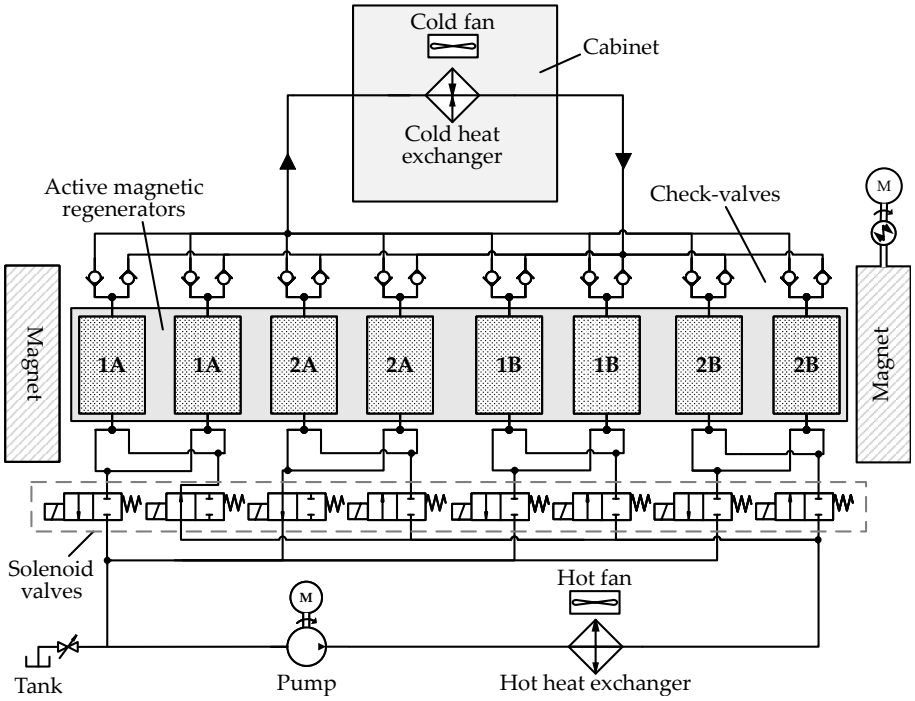

Figure 3. Schematic representation of the HC.

The solenoid valves have a nominal power consumption of 1.5 W, a flow coefficient of 0.3 $m^3\ h^{-1}$ and a maximum magnet frequency of 1 Hz. The pump is a microgear type and was selected following a broad search and tests of pump models. The pump was experimentally evaluated and the curves are presented in Fig. 4, showing the pump flow rate and the system load curve as a function of the pressure difference. The nominal supply voltage of 24 V was modulated by a pulse width modulator (PWM) and the colors represent the PWM percentages varying from 20 to 100%. The system load curve was estimated numerically.

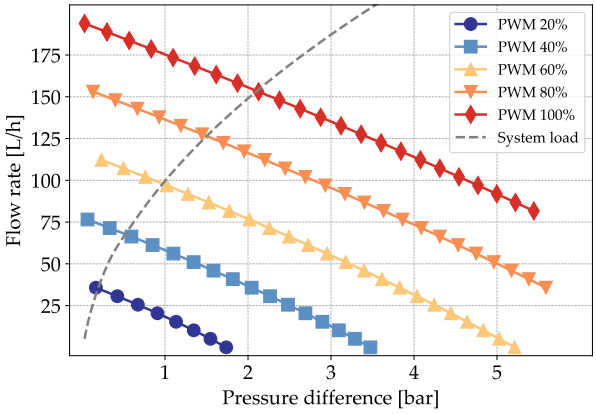

Figure 4. Experimental curve of flow rate as a function of the pressure difference.

2.4 Heat Exchangers and Fans

The HEx of the MR2 are responsible for connecting the magnetic refrigeration unit to the thermal reservoirs. Both cold- and hot-side heat exchangers (CHEx and HHEx) are finned-tube type and assisted by compact fans. In MR1, the fans were the second most consuming components in the operation point. Thus, the aim of the HEx design was to find optimized CHEx and HHEx that would minimize the total fan power consumption in MR2. The main design parameters of the CHEx and HHEx and the respective fan power consumption are presented in Tab. 3.

Table 3. Dimensions and parameters of the HEx and fans.

Parameter	Value	Parameter	Value
Tube diameter	9.5 mm	No. of longitudinal tubes	2
Tube thickness	0.3 mm	No. of transverse tubes	9
Fin thickness	0.18 mm	CHEx Width	250 mm
Fin density	0.63 fin mm^{-1}	HHEx Width	350 mm
Transverse tube pitch	25.4 mm	Cold fan power	2 W
Longitudinal tube pitch	22 mm	Hot fan power	3 W

Both HEx were manufactured following the optimized design parameters of Tab. 3. The cold fan has a nominal power of 2 W and an air flow of 114 m^3 h^{-1} and the hot fan has a nominal power of 3.2 W and an air flow of 140 m^3 h^{-1}. Figure 5 shows the effectiveness curve of both CHEx and HHEx as a function of the liquid stream flow rate.

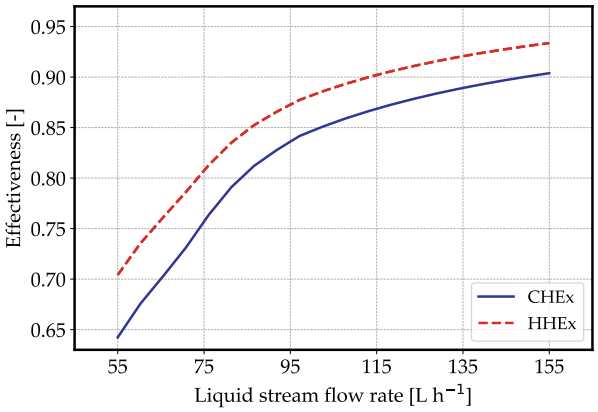

Figure 5. Numerical effectiveness curves as a function of the liquid stream flow rate for the hot and cold HEx.

2.5 Cabinet

The MR2 cabinet is a retrofit from VC1, where the original refrigerant circuit was replaced by a simpler configuration, with a single loop and one compartment. The cabinet has 150 L of internal volume, 500 mm of width, 970 mm of height

and 595 mm of depth. The cabinet walls are composed of a liner made of high-impact polystyrene (HIPS), a thermal insulation made of expanded polyurethane with cyclopentane (PU C-Pentane) and an external steel plate.

The overall thermal conductance (UA) of the cabinet was experimentally determined to estimate the thermal load imposed by the surroundings at the operation point and calculate the target cooling capacity of MR2. Figure 6 presents the experimental UA as a function of the power input in the cold fan. With the increase in the power supply of the cold fan, the air velocity inside the cabinet increases, enhancing the heat transfer and increasing the cabinet UA.

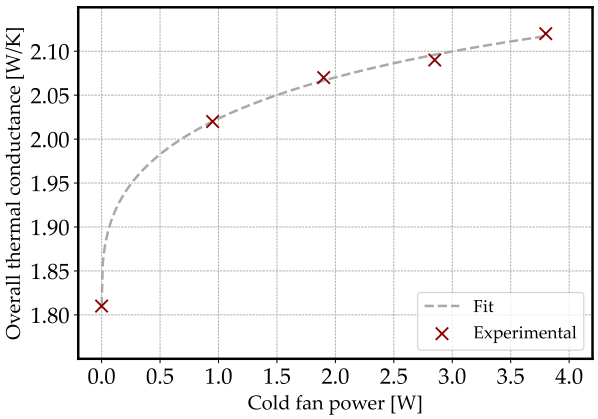

Figure 6. Overall thermal conductance of the cabinet as a function of the fan power.

2.6 Overview

The main components of the previously described subsystems are assembled in a magnetic cooling unit (MCU), which contains the MC, the AMR and the HC. The CHEx and cold fan are assembled inside the cabinet and the HHEx and the hot fan are assembled at the rear of the cabinet. Other components such as controls and electrical instrumentation are also assembled at the rear of the cabinet. The components were positioned inside the MCU focusing on minimizing the utilized volume. Figure 7 shows a schematic view of the MCU coupled with the wine cooler cabinet, forming the MR2. The MCU is expected to occupy an extra 40% of the cabinet volume.

Figure 7. Schematic representation of the MCU coupled to the wine cooler cabinet.

3. PERFORMANCE METRICS

To evaluate the performance of the MR2 system, first- and second-law based performance metrics were analyzed, in terms of COP and $\eta_{2\mathrm{nd}}$. The COP is the ratio between the cooling capacity ($\dot{Q}_\mathrm{c}$) to the total power consumption ($\dot{W}_\mathrm{tot}$),

and is calculated as in Eq. (1). The $\eta_{2\text{nd}}$ is the ratio of the COP to the Carnot COP, COP_{Carnot}, and is calculated as in Eq. (2).

$$COP = \frac{\dot{Q}_{\text{c}}}{\dot{W}_{\text{tot}}} \tag{1}$$

$$\eta_{2\text{nd}} = \frac{COP}{COP_{\text{Carnot}}} \tag{2}$$

The steady state cooling capacity is equal to the the thermal load imposed by the surroundings to the cabinet walls plus the power consumption of cold fan ($\dot{W}_{\text{cf}}$):

$$\dot{Q}_{\text{c}} = UA\,(T_{\text{sur}} - T_{\text{cab}}) + \dot{W}_{\text{cf}} \tag{3}$$

where T_{sur} and T_{cab} are the temperatures of the surroundings and the cabinet, respectively. The total power consumption of MR2 is calculated as the sum of the power contributions of each subsystem, according to Eq. (4). The power consumption of the magnet motor ($\dot{W}_{\text{m}}$) is estimated as the sum of the magnetic power and the power due to magnetic interactions in the MC. The efficiency of the transmission was estimated as 80%. The power of the pump ($\dot{W}_{\text{p}}$), the solenoid valves ($\dot{W}_{\text{v}}$) and the fans ($\dot{W}_{\text{f}}$) are calculated by the estimation of the electrical power. Both $\dot{W}_{\text{p}}$ and $\dot{W}_{\text{v}}$ were calculated with experimental data and $\dot{W}_{\text{f}}$ was calculated with catalogue data.

$$\dot{W}_{\text{tot}} = \dot{W}_{\text{m}} + \dot{W}_{\text{p}} + \dot{W}_{\text{v}} + \dot{W}_{\text{f}} \tag{4}$$

Lastly, COP_{Carnot} is calculated as the ratio of the cabinet temperature to the temperature difference between the hot and cold reservoirs:

$$COP_{\text{Carnot}} = \frac{T_{\text{cab}}}{T_{\text{sur}} - T_{\text{cab}}} \tag{5}$$

4. NUMERICAL RESULTS

The numerical results of MR2 were characterized in the form of steady state performance maps as functions of the input variables. The input variables were the flow rate (55 to 155 L h^{-1}) and the rotating frequency of the magnet (0.25, 0.50, 0.75 and 1.00 Hz). The temperature of the surroundings was kept fixed at 25°C. The blow fraction was fixed at 25%[2]. Figure 8 presents the results of the cabinet temperature as a function of the flow rate and frequency. As it can be seen, the target cabinet temperature of 12°C is reached for all magnet frequencies, with flow rates ranging from 75 to 90 L h^{-1}. The minimum cabinet temperature is around 10°C, for both the frequencies of 0.75 and 1.00 Hz and for a flow rate of 155 L h^{-1}. The curve trends indicate points of minimum temperatures for each magnet frequency. For the frequencies of 0.25 and 0.5 Hz, the limits are reached for the flow rates of around 115 and 140 L h^{-1}, respectively. For the frequencies of 0.75 and 1.00 Hz, the limit flow rate of 155 L h^{-1} is approaching the points of minimum temperature. The curve trends also indicate a limit in the available cooling capacity with the increase of the frequency, as the 1.00 Hz curve contributes very little to the decrease of cabinet temperature when compared to the 0.75 Hz curve. With the present system layout and its limits, the maximum expected temperature span reachable by MR2 is around 15°C.

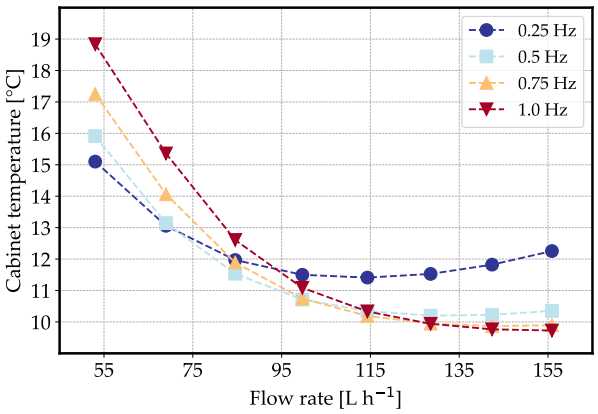

Figure 8. Numerical results of cabinet temperature as a function of the flow rate and frequency.

[2]The blow fraction is the fraction of ratio of the blow period in one regenerator and the cycle period.

Figures 9 and 10 present the numerical results of COP and $\eta_{2\mathrm{nd}}$, respectively, as a function of the flow rate and frequency. The highest overall performance of MR2 was achieved for a flow rate of 70 L h^{-1} and a frequency of 0.25 Hz, in which the cabinet reached a temperature of 13°C for a COP of 1.46 and a $\eta_{2\mathrm{nd}}$ of 6.77%. Additionally, MR2 is expected to reach a cabinet temperature of 10°C with a COP of 0.57 and a $\eta_{2\mathrm{nd}}$ of 3.51%, for a flow rate of 155 L h^{-1} and frequency of 0.75 Hz. Considering the target temperature and in consonance with the MR2 design goals, the operation point of the system was selected focusing on the system performance. Evaluating the performance maps, the test point that reached the target cabinet temperature of 12°C with the highest performance was the one with a flow rate of around 85 L h^{-1} and frequency of 0.25 Hz. Thus, the operation point has a COP of 1.32 and a $\eta_{2\mathrm{nd}}$ of 6.76%.

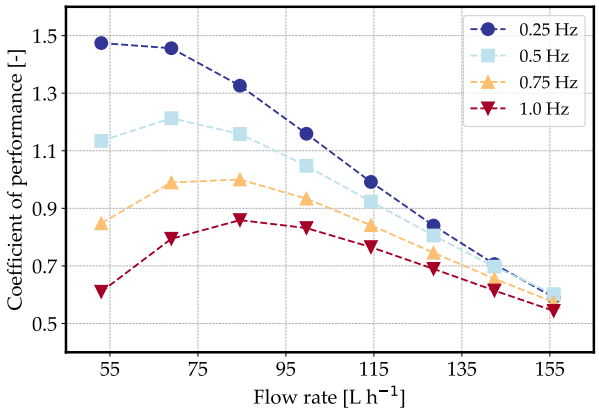

Figure 9. Numerical results of COP temperature as a function of the flow rate and frequency.

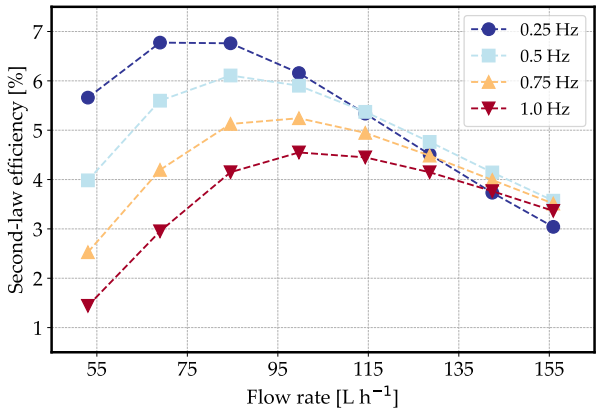

Figure 10. Numerical results of $\eta_{2\mathrm{nd}}$ as a function of the flow rate and frequency.

To assess the contributions of each subsystem to the system power consumption, Fig. 11 presents the breakdown of power consumption for a fixed frequency of 0.5 Hz and different flow rates (55, 100 and 155 L h^{-1}) and Fig. 12 presents the breakdown of power consumption for a fixed flow rate of 70 L h^{-1} for all magnet frequencies. For a fixed frequency, the increase of flow rate results in a great increase of the total power consumption. The major contribution to this increase is the power consumption of the pump, going from the least consuming subsystem to the most consuming one. The contribution of the magnet motor to the power consumption also increases with the flow rate, due to the increase in the magnetic work. The power of the solenoid valves do not vary with the flow rate and the power of the fans is fixed at 5 W. For a fixed flow rate, the increase of the total power consumption with the frequency is not so significant. The major contribution to the total power consumption increase are the solenoid valves, as they are actuated more often. The power consumption of the motor slightly decreases with the increase of the frequency, as the torque requirement also decreases. The pump power consumption does not change with the frequency.

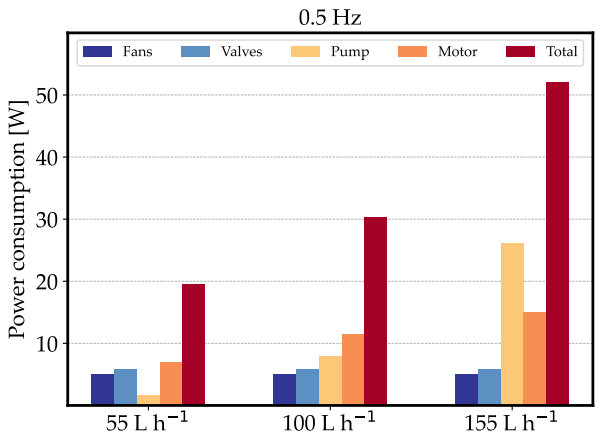

Figure 11. Power consumption breakdown for a fixed frequency of 0.5 Hz.

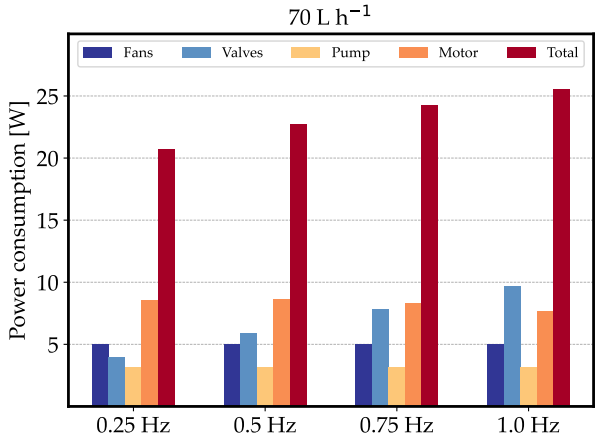

Figure 12. Power consumption breakdown for a fixed flow rate of 70 L h^{-1}.

Carrying out a further analysis on the operation point, Fig. 13 presents the breakdown of the power consumption percentage for a flow rate of 85 L h^{-1} and a frequency of 0.25 Hz. The driving motor of the MC is the most consuming

subsystem, followed by the pump, the fans and the solenoid valves. The pump contributes to only 21.9% of the total power consumption of the operation point, which is a very different result compared with the MR1 system. The operation point of the MR1 system had a flow rate of 125 L h^{-1} and a magnet frequency of 0.5 Hz, and the pump contributed to more than 50% of the total power consumption, reaching 36 W. For the MR2 operation point, the pump consumes less than 6 W. The low contribution of the pump to the total power consumption of the MR2 reflects both that the pumping system is well sized for the operation point and that the new hybrid matrix of the solid refrigerant increased the cooling capacity of the AMR for the MR2 system. The contribution of the fans also decreased, going from 12 W in MR1 to 5 W in MR2, reflecting the optimization of the heat exchangers.

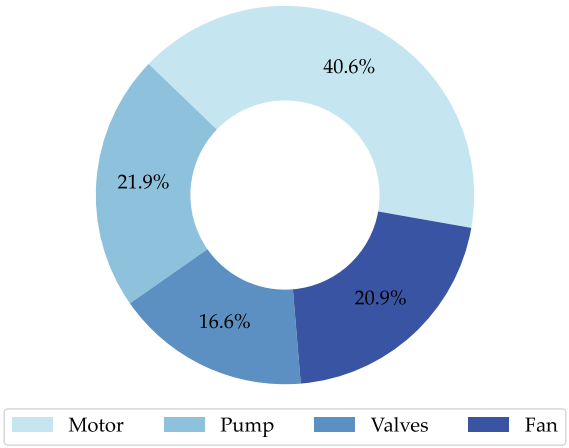

Figure 13. Power consumption breakdown for the operation point (85 L h^{-1} and 0.25 Hz).

As one of the main goals of the MR2 design was to outperform both MR1 and VC1, Fig. 14 presents the comparison of the performance metrics for the three systems for a cabinet temperature of 12°C and an ambient temperature of 25°C. The COP of MR2 is expected to be 170% higher than MR1 (0.49) and 89% higher than VC1 (0.7). The η_{2nd} of MR2 is expected to be 238% higher than MR1 (2.00%) and 116% higher than VC1 (3.13%).

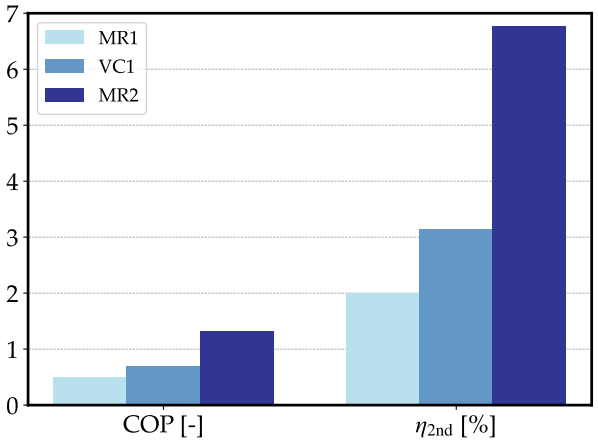

Figure 14. Performance comparison of the MR1, VC1 and MR2 cooling systems when operating the same wine cooler cabinet, for an ambient temperature of 25°C and a cabinet temperature of 12°C.

5. CONCLUSIONS

In this work, the design and numerical results of a novel compact magnetocaloric refrigeration system were presented and discussed. The main goals for the magnetocaloric system were to outperform a similar vapor compression system when operating the same wine cooler cabinet and to be more compact than its previous prototype version. The numerical results indicate that the magnetocaloric system can outperform the vapor compression system by 116% in terms of the second-law efficiency for the target cabinet temperature of 12°C. Furthermore, the magnetocaloric system is expected to outperform its previous prototype version by 238% while employing 48.5% less mass of magnet.

The increase in the performance of the novel magnetocaloric wine cooler in comparison with its previous prototype version can be attributed to some key design aspects. First, it reflects the increase in the AMR cooling capacity, obtained with the use of a hybrid matrix of Gd and La-Fe-Si alloys rather than using only Gd and Gd-Y. Second, it echoes the optimization of the components for the operation point, specially the pump and the heat exchangers, which decreased considerably the overall power consumption of the novel system. The design phase of the PoloMag project is completed and the magnetocaloric wine cooler is currently being commissioned. Further steps will include the experimental characterization of the system and the development of control strategies to enhance overall system performance.

6. ACKNOWLEDGEMENTS

This work was partially funded by the INCT (National Institutes of Science and Technology) Program, CNPq, FAPESC and CAPES. Financial support from EMBRAPII, NIDEC GA (formerly Embraco) and CODEMGE is also acknowledged.

7. REFERENCES

Aprea, C., Cardillo, G., Greco, A., Maiorino, A. and Masselli, C., 2016. "A rotary permanent magnet magnetic refrigerator based on AMR cycle". *Applied Thermal Engineering*, Vol. 101, pp. 699–703.

Cardoso, P.O., Destro, M.C., Alvares, M.G., Lozano, J.A., Negri, V.J.D. and Barbosa Jr., J.R., 2016. "Modeling of a novel digital hydraulic system for a magnetic refrigerator". In *Proceedings of the Seventh IIF-IIR International Conference on Magnetic Refrigeration at Room Temperature*. Torino, Italy.

Dall'Olio, S., Masche, M., Liang, J., Insinga, A.R., Eriksen, D., Bjørk, R., Nielsen, K.K., Barcza, A., Vieyra, H.A., Beek, N.V., Bez, H.N., Engelbrecht, K. and Bahl, C.R., 2021. "Novel design of a high efficiency multi-bed active magnetic regenerator heat pump". *International Journal of Refrigeration*, Vol. 132, pp. 243–254.

De Sá, N.M., Nakashima, A.T.D., Pagnan, E., Lorenzoni, A., Luz, G.M., Hoffmann, G., Peixer, G.F., Lozano, J.A. and Barbosa, J.R., 2023a. "PoloMag Project: Designing a compact magnetocaloric wine cooler." In *Proceedings of the 26th International Congress of Refrigeration (in press)*. Paris, France.

De Sá, N.M., Nakashima, A.T., Lozano, J.A. and Barbosa, J.R., 2023b. "Thermodynamic comparison of magnetocaloric and vapor compression wine coolers". *International Journal of Refrigeration*, Vol. 156, pp. 29–39.

Engelbrecht, K., Eriksen, D., Bahl, C.R., Bjørk, R., Geyti, J., Lozano, J.A., Nielsen, K.K., Saxild, F., Smith, A. and Pryds, N., 2012. "Experimental results for a novel rotary active magnetic regenerator". *International Journal of Refrigeration*, Vol. 35, No. 6, pp. 1498–1505.

Eriksen, D., Engelbrecht, K., Bahl, C.R., Bjørk, R., Nielsen, K.K., Insinga, A.R. and Pryds, N., 2015. "Design and experimental tests of a rotary active magnetic regenerator prototype". *International Journal of Refrigeration*, Vol. 58, pp. 14–21. ISSN 01407007. doi:10.1016/j.ijrefrig.2015.05.004.

Jacobs, S., Auringer, J., Boeder, A., Chell, J., Komorowski, L., Leonard, J., Russek, S. and Zimm, C., 2014. "The performance of a large-scale rotary magnetic refrigerator". *International Journal of Refrigeration*, Vol. 37, No. 1, pp. 84–91.

Kaneko, G.H., Souza, A.C., Moro, F., Colman, F.C., Conceição, W.A., Alves, C.S. and Trevizoli, P.V., 2019. "Design and assembling of a magnetic circuit for a thermomagnetic motor apparatus". *Journal of the Brazilian Society of Mechanical Sciences and Engineering*, Vol. 41.

Nakashima, A.T., Peixer, G.F., Lozano, J.A. and Barbosa, J.R., 2022. "A lumped-element magnetic refrigerator model". *Applied Thermal Engineering*, Vol. 204.

Nakashima, A.T., Fortkamp, F.P., de Sá, N.M., dos Santos, V.M., Hoffmann, G., Peixer, G.F., Dutra, S.L., Ribeiro, M.C., Lozano, J.A. and Barbosa, J.R., 2021. "A magnetic wine cooler prototype". *International Journal of Refrigeration*, Vol. 122, pp. 110–121.

Pagnan, E., 2022. "Projeto de um circuito magnético para um protótipo de refrigeração magnetocalórica visando redução de custos e facilidade de fabricação." *Undergraduate thesis - Federal University of Santa catarina*.

Peixer, G.F., Silva, M.C., Lorenzoni, A., Hoffmann, G., dos Santos, D., do Rosário, G.M., Pagnan, E., Teza, H.F., Silva, P.M., Dutra, S.L., Ribeiro, M.C., Rosa, M.A., Döring, A., Vieira, B.P., Nakashima, A.T., Wendhausen, P.A., Teixeira, C.S., Lozano, J.A. and Barbosa, J.R., 2023. "A magnetocaloric air-conditioning system prototype". *International Journal of Refrigeration*.

Qian, S., Nasuta, D., Rhoads, A., Wang, Y., Geng, Y., Hwang, Y., Radermacher, R. and Takeuchi, I., 2016. "Not-in-kind cooling technologies: A quantitative comparison of refrigerants and system performance". *International Journal of Refrigeration*, Vol. 62, pp. 177–192.

Tura, A. and Rowe, A., 2011. "Permanent magnet magnetic refrigerator design and experimental characterization". *International Journal of Refrigeration*, Vol. 34, No. 3, pp. 628–639.

8. RESPONSIBILITY NOTICE

The authors are solely responsible for the printed material included in this paper.